Annals of Anatomy 262 (2025) 152699

Contents lists available at ScienceDirect

Annals of Anatomy

journal homepage: www.elsevier.com/locate/aanat

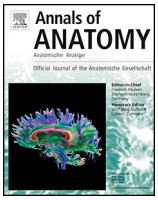

Morphological and immunological approach for studying the distribution pattern of mitochondria and germ granules during oogenesis of the guppy (*Poecilia reticulata*)

Giovanni Piccinini [1], Mariangela Iannello [1], Maurizio Lazzari, Pietro Cacialli, Valeria Franceschini, Maria Gabriella Maurizii [2], Liliana Milani [2,3,*]

Department of Biological, Geological and Environmental Sciences (BiGeA), University of Bologna, Bologna, Italy

ARTICLE INFO

Keywords:
Immunolocalization
Vasa
TOMM20
PLD6
TDRD7
TDRKH
TEM

ABSTRACT

A same set of genes is associated to germline determination and differentiation in almost all Metazoa. Previous studies in several animals, also from distantly related taxa, showed a close association between germline determinants in germ granules and mitochondria, with observations at transmission electron microscopy and immunological approaches. However further investigations are needed to document their respective distribution and elucidate the role of mitochondria in the process of germ granule formation. In the present study we used an emerging animal model to study germline differentiation, *Poecilia reticulata*, also known as guppy, and different experimental approaches: western blot, immunolocalization, and transmission electron microscopy to investigate the distribution of mitochondria and germ granules during oogenesis. We used anti-Vasa, anti-TDRKH, and anti-TDRD7 to label germline markers, anti-TOMM20 to localize mitochondria, and anti-PLD6 to highlight germline mitochondria. Our observations in previtellogenic oocytes support the co-participation of the nucleus and mitochondria in the production of germ plasm-related material. In previtellogenic oocytes, immunodetection revealed the presence of the germline markers and PLD6 staining in the perinuclear area. The most striking evidence is the observation in the same cell type of plume-shaped structures that at electron microscopy appear as formed by mitochondrial aggregates intermingled with electron-dense germ granules distributed around the nuclear envelope. Overall, our results support the close association between germ granule and mitochondria during germline differentiation, strengthening the foundations for further insights.

1. Introduction

A metazoan-wide conserved gene set (germline multipotency program, GMP) is required for germline specification and gamete differentiation (Ewen-Campen et al., 2010; Juliano et al., 2010). These factors show highly conserved molecular interactions (Shukalyuk and Isaeva, 2012) and are often organized in macromolecular cytoplasmic structures of ribonucleoproteic composition. These germ-plasm related structures can differ between species, sexes, and germ cell differentiation stages (Voronina et al., 2011), and in the present paper we refer to them as germ granules. These granules can be identified by Transmission Electron Microscopy (TEM) as a cloud-like electron-dense granulofibrillar material, are positioned in the perinuclear region or scattered in the cytoplasm of germ cells and can be associated with mitochondria depending on the stage of germ cell differentiation (Matova and Cooley, 2001). Germ granules are fundamental for germ fate acquisition, and the removal of individual germ plasm components is sufficient to trigger somatic differentiation of primordial germ cells in many animal models (reviewed in Gross-Thebing et al., 2017).

GMP genes can be found in germ granules of different species, either as transcripts or protein products, and most of them are associated with transcriptional and, more often, post-transcriptional regulation. *Vasa*, a DEAD-box RNA helicase, probably the most famous GMP gene, has been studied in many animals, including teleosts, such as zebrafish (Olsen

* Corresponding author.
E-mail address: liliana.milani@unibo.it (L. Milani).
[1] share first authorship
[2] share senior authorship
[3] orcid ID: 0000–0001-5052–2075

https://doi.org/10.1016/j.aanat.2025.152699
Received 9 April 2025; Received in revised form 26 June 2025; Accepted 17 July 2025
Available online 18 July 2025

et al., 1997), medaka (Shinomiya et al., 2000), tilapia (Kobayashi et al., 2000), and recently *Poecilia reticulata* (Milani et al., 2022). The product of this gene acts as a post-transcriptional regulator and interact with many other germline determinants. A whole set of Tudor domain-containing proteins with multiple protein-protein interaction domains functions as scaffold-like recruiting platforms acting on the supramolecular stability of germ granules themselves (Seydoux and Braun, 2006; Siomi et al., 2010; Pek et al., 2012; *Danio rerio*, Huang et al., 2011b). For instance, TDRD7 is involved in the proper assembly of germ granules in *Drosophila melanogaster* (Patil et al., 2014), in *Mus musculus* (Tanaka et al., 2011), and in *D. rerio* (Strasser et al., 2008; D'Orazio et al., 2021). TDRKH is instead involved in the recruitment of Piwi, a key component of the piRNA-dependent pathway of retrotransposon silencing (Thomson and Lin, 2009; Juliano et al., 2010): in zebrafish, *piwi*-like genes impairment is associated with germ cell apoptosis and lack of germ cell differentiation and meiosis (Houwing et al., 2007, 2008). The mitochondrial surface is one of the places where piRNA biogenesis is thought to occur in many species, at the level of the intermitochondrial cement, a prominent germ granule that locates among aggregated mitochondria in mammalian germ cells (Ding et al., 2019), described also in other animals, as fish (e.g. *Labeobarbus marequensis*, Zelazowska and Halajian, 2019).

Phospholipase D6 (PLD6, or MitoPLD) is typically localized in the outer mitochondrial membrane, acts in piRNA biogenesis and germ cell differentiation, and is expressed in mammalian germ cells of both sexes (Aravin and Chan, 2011; Watanabe et al., 2011; Nishimasu et al., 2012; Kabayama et al., 2017; Izumi et al., 2020). The protein is known to regulate fusion/fission dynamics of the mitochondrial network by producing the lipid messenger phosphatidic acid (Huang et al., 2011a). In zebrafish, *pld6* mRNA was observed exclusively in germ cells of both sex juveniles, thus being considered a germline marker, with a direct association to fertility (Zhang et al., 2022).

In several animals, material released from mitochondria is involved in germ granule formation and germline maintenance. In *Mus musculus* and *Ruditapes philippinarum*, dense granules released from mitochondria have been observed (Reunov, 2006; Reunov et al., 2019; respectively), and Vasa protein has been localized within mitochondria (Reunov and Reunova, 2015; Reunov et al., 2021; respectively). All this considered, the distribution of mitochondria and germ granules suggests their molecular interaction during germline development of many animals.

The guppy *P. reticulata* (Actinopterygii, Neoteleostei, Cyprinodontiformes) is one of the most studied viviparous fish due to its reproductive mode and for the peculiar histological organization (Campuzano-Caballero and Uribe, 2014). A distinctive feature of almost all viviparous teleosts occurs when, during the early embryonic development, the right and left ovaries fuse, forming a single ovary (Uribe et al., 2019). The single ovary of *P. reticulata* is of the cystovarian type and in cross or longitudinal sections at the level of central lumen, different stages of germ cells are observable: from oogonia located in the germinal epithelium, to previtellogenic or vitellogenic oocytes scattered in the ovarian stroma. For such features, *P. reticulata* can be a good neoteleostean model to study expression and distribution of germline determinants during germ cell differentiation.

In the present study, we investigated with morphological and immunological approach the distribution of mitochondria and germ granules during oogenesis of the guppy (*Poecilia reticulata*). We analyzed the expression patterns of some GMP factors in relationship to the localization of mitochondria by using antibodies for germline determinants (anti-Vasa, anti-TDRKH, and anti-TDRD7) and antibodies for mitochondria (anti-TOMM20, a constitutive subunit of the mitochondrial translocase of the outer membrane, and anti-PLD6). The results obtained help to understand how germline determinants and mitochondria are concurrently involved in some phases of germline differentiation.

2. Material and methods

2.1. Primary antibodies

Commercial antibodies were used to immunolocalize Vasa (ab27591; monoclonal; Abcam), TDRKH (GTX129795; polyclonal; GeneTex), TDRD7 (ab224462; polyclonal; Abcam), TOMM20 (mAb-4F3; monoclonal; Merck), and PLD6 (ab237612; polyclonal; Abcam). The antibodies were developed in rabbit (polyclonal antibodies) or mouse (monoclonal antibodies) against human epitopes.

We checked for full-length gene presence of *vasa*, *tdrkh*, *tdrd7*, *tomm20* and *pld6* in *P. reticulata* proteome (from NCBI: GCF_000633615.1). Once retrieved, annotated sequences from the proteome (based on annotation nomenclature), were used to calculate the predicted molecular weights with online tools (https://www.bioinformatics.org/sms/prot_mw.html). An alignment of the protein sequences carried out using "BLASTp" (Altschul et al., 1990) (NCBI) allowed us to evaluate amino acid sequence conservation between *P. reticulata* and *Homo sapiens*, the latter being the species from which polypeptides were used as immunogens to produce primary antibodies. This was done prior to immunolocalization to assure the presence in *P. reticulata* orthologues of the region against which the antibody was produced.

2.2. Animals

All procedures conformed to the guidelines of European Communities Council Directive (86/609/CEE), the current Italian legislation regarding the use and care of animals, and the guidelines issued by the US National Institutes of Health. This study was approved by the Scientific Ethics Committee of the University of Bologna (protocol no. 17/79/2014).

2.3. Western blot

For immunoblotting, homogenates from four ovaries were produced and SDS-PAGE carried out following Milani et al. (2022). Proteins were transferred to a Hybond-ECL membrane (Amersham International, Buckinghamshire, UK). Non-specific protein-binding sites were blocked with 5 % dried skimmed milk (Bio-Rad Laboratories, Hercules, CA, USA), 3 % bovine serum albumin (BSA) (Sigma), 0.1 % Tween 20 (Tw) (Sigma) in Tris Buffered Saline solution (TBS: 200 mM Trizma base; 137 mM NaCl), for 1 h 30 min, at room temperature (RT), and subsequently washed with TBS- 0.1 % Tw. Membranes were then incubated overnight (ON) at 4 °C and for 1 h 15 min at RT with the primary antibodies diluted in TBS-0.1 % Tw, pH 7.4 (anti-Vasa 1:200; anti-TDRKH 1:1000; anti-TDRD7 1:500; anti-TOMM20 1:200; anti-PLD6 1:2000). After rinsing, membranes were incubated with secondary antibodies conjugated with horseradish peroxidase (sc-2055 goat anti-rabbit for polyclonal antibodies and sc-2004 goat anti-mouse for monoclonal ones; Santa Cruz Biotechnology Inc., Santa Cruz, CA, USA) at the dilution of 1:5000 for 1 h at RT. The washed membranes were treated with ECL Western Blotting Detection Reagents (GE Healthcare) and exposed to Hyperfilm ECL (GE Healthcare).

2.4. Immunolocalization

Ovaries of ten adult *P. reticulata* females were rapidly dissected and fixed with 3.7 % paraformaldehyde + 0.25/0.5 % glutaraldehyde (depending on gonads dimension) in a buffer containing 80 mM KPIPES,

1 mM $MgCl_2$, 5 mM EGTA, and 0.2 % Triton X-100 (Tx), pH 6.8, for 4 h at RT. Fixed ovaries were washed with PBS (pH 7.2) for 1 h and embedded in 7 % agar. Vibratome sections (Leica VT1000 S), were post-fixed with increasing concentrations of methanol (50–100 %) and rehydrated in PBS or TBS (10 mM Tris–HCl, 155 mM NaCl; pH 7.4). Unreacted aldehydes were reduced with 70 mM sodium borohydride ($NaBH_4$) in TBS (pH 7.4) for 90 min at RT, followed by several washes with TBS-0.1 %Tx for 2 h. Permeabilization was carried out by adding TBS-1 %Tx to the sections and leaving the tissues ON at 4 °C. Then, free-floating sections were processed for immunofluorescence as described below.

Non-specific protein-binding sites were blocked in TBS-0.1 %Tx with 1 % BSA and 10 % NGS (pH 7.4) for 1 h 30 min at RT. Primary antibodies were diluted in TBS-0.1 %Tx with 3 % BSA (pH 7.4) and sections were incubated for 60 h at 4°C (anti-Vasa 1:70 and anti-TDRKH 1:50, as in Milani et al., 2022; anti-TDRD7 1:100; anti-TOMM20 1:50; anti-PLD6 1:200). After washing, the treated sections were incubated with polyclonal antibodies (goat anti-rabbit for polyclonal antibodies; goat anti-mouse for monoclonal ones) conjugated with Alexa Fluor 488 diluted 1:400 in TBS-0.1 %Tx with 1 % BSA and 1 % NGS for 24 h at 4°C. All immunolabeled sections were then washed and stained with a nuclear dye: 1 μM TO-PRO-3 iodide (Molecular Probes) in PBS (pH 7.2) for 10 min at RT. Sections were then washed and mounted in anti-fade mounting medium (2.5 % DABCO, (Sigma), 50 mM Tris (pH 8), and 90 % glycerol). Finally, the sections were covered with coverslips, sealed with nail polish and stored at 4°C in the dark. Controls were performed using sections from which the first antibody was replaced with 1 % NGS in TBS-0.1 % Tx. Such controls showed a very faint background noise, together with the signal of some cells well recognizable as erythrocytes known to show a characteristic autofluorescence. Sections were examined with Leica TCS SL confocal laser scanning microscope equipped with Ar/He/Ne lasers. Objective lens used were 40x/0.75 PH2 and 63x/1.32–0.6 OIL CS, and images were acquired with Leica confocal software.

Some sections were treated for hematoxylin-eosin to clarify tissue morphology and for immunohistochemistry to complement immunofluorescence detections (protocols as in Milani et al., 2022). In this case, sections were examined with Olympus BH-2. Objective lens used were 4x NA 0.10 (DPlan; 160/0.17), 20x NA 0.46 (SPlan; 160/0.17), using BEL BlackL 5000 digital camera. Images were acquired with BELL Eurisko™ software.

2.5. Transmission electron microscopy (TEM)

For TEM analysis, ovaries were quickly dissected from three females of *P. reticulata*, deeply anesthetized with 0.1 % 3-aminobenzoic acid ethyl ester (Sigma). Samples were immersion-fixed in 2 % paraformaldehyde and 2.5 % glutaraldehyde in 0.1 M cacodylate buffer (pH 7.4) for 24 h at 4 °C. After overnight wash in 0.1 M cacodylate buffer, pH 7.4, at 4 °C, the gonads were postfixed in 1 % osmium tetroxide in the same buffer for 1 h at 4 °C. Samples were then washed in 0.1 M cacodylate buffer, pH 7.4, dehydrated in a graded series of acetone (50, 70, 90, and 100 %) and embedded in Durcupan ACM (Fluka, Buchs, CH). Samples were cut on a Reichert U3 ultramicrotome. Semithin sections, 0.5–1 μm thick, were stained with toluidine blue and examined by light microscope to identify the area of interest. Thin sections collected on formvar-coated copper grids were stained with uranyl acetate and lead citrate solutions and examined in a CM 100 Philips electron microscope operating at 80 kV, images were acquired with Olympus Megaview G2, using iTEM FEI software.

3. Results

Sequence analysis supports highly conserved protein sequence portions between antigenic sites used for *H. sapiens* against the homologous regions in *P. reticulata* (Table 1).

Table 1
Summary statistics of the alignments between antigenic sites used for *H. sapiens* against the homologous regions in *P. reticulata*.

Query	E value	% identity
Human TDRD7 aa 750–950	3×10^{-34}	31.88
Human TDRKH (center region; proprietary exact sequence)	3×10^{-124}	39.58
Human DDX4/ MVH (VASA) aa 700-C-terminus	0.033	66.67
Human PLD6 full length	6×10^{-39}	48.92
Human TOMM20 full length	1×10^{-84}	83.45

Antibody specificity was also supported by Western blots. However, Vasa SDS-PAGE of female homogenates was hampered by the abundant presence of yolk proteins, which appear as a high molecular weight aggregate (visible in Coomassie staining; data not shown); thus, for this marker we esteemed the molecular weight from WB obtained from male homogenates (Fig. 1). Even if the weight corresponds between sexes, we show WB for male and female samples also for TDRDKH, since in females the band was particularly faint (Fig. 1). Anti-Vasa ab27591 antibody revealed a single band in both female and male samples, ~70 kDa in males, consistent with the predicted weight of the protein (69.9 kDa). TDRKH molecular weight for female samples was consistent with results obtained for *P. reticulata* male samples with the same anti-TDRKH polyclonal antibody in Milani et al. (2022), with a band coherent with the predicted of ~63 kDa. TDRD7 in *P. reticulata* has a predicted weight of 132.69 kDa. Referring to the protein standard used, anti-TDRD7 detected a band (~120 kDa) close to the expected weight, but an additional band of ~55 kDa was also observed. Tudor protein bands were quite faint even when using homogenates at high protein concentration. Anti-TOMM20 antibody detected a molecular weight band of ~20 kDa (predicted 16.47 kDa); non-specific bands with higher molecular weight are also present. Anti-PLD6 antibody showed one band at ~55 kDa (predicted 23.38 kDa) as well as some faint, probably non-specific high molecular weight bands.

3.1. Histological organization of the ovary

With hematoxylin-eosin staining we observed ovary morphology (Fig. 2). The single ovary of *P. reticulata* consists of germinal epithelium, ovarian follicles, and stroma. The ovary shows an internal lumen, lined by the germinal epithelium which forms numerous and irregular folds which extend into the lumen (Fig. 2a, b). The germinal epithelium contains groups of oogonia and of early oocytes surrounded by somatic cells (Fig. 2b). Previtellogenic oocytes grow within ovarian follicles (Fig. 2). Each ovarian follicle consists of a single oocyte surrounded by somatic follicular cells, basal lamina, and somatic thecal cells. This organization is visible in immunostained sections and in ultrathin sections at TEM.

3.2. Immunolocalization of germline determinants

In general, germ cells are characterized by a larger nucleus than somatic cells and the stained chromatin helped us to identify the stages of germ cells in immunofluorescence analyses. In bigger oocytes, we often fail to observe nuclear labeling, although we can still identify the nucleus due to the absence of background noise. Germ cells were identified for size, morphology, position, and presence of lipid droplets (following Uribe et al., 2019). The Vasa staining was also used to identify germ cells, being *vasa* expression considered a germline specific marker in fish (e.g. *D. rerio*, Hartung et al., 2014; *Sebastes schlegelii*, Zhou et al., 2020; *Oryzias celebensis*, Chen et al., 2022; *Plectropomus leopardus*, Wang et al., 2022). Somatic cells were not marked with the used antibodies against germline determinants. The small cells with bright nuclei and red autofluorescence are erythrocytes (Shrirao et al., 2021).

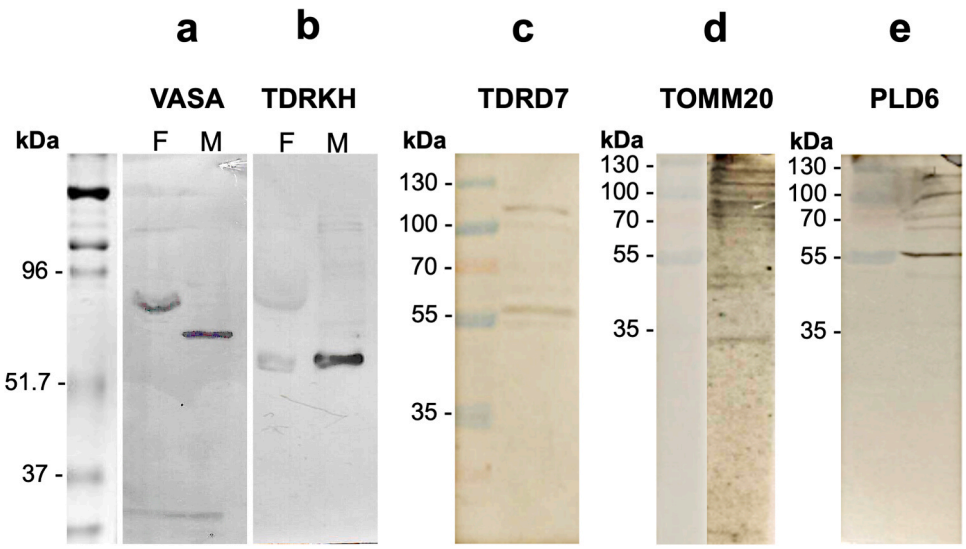

Fig. 1. Western blot. a) Anti-VASA; (b), anti-TDRDKH; (c) anti-TDRD7; (d) anti-TOMM20; (e) anti-PLD6. For each WB the first lane on the left represents the protein standard. In the case of Vasa and TDRKH both homogenates of female and male gonads were used given the interference with run due to yolk.

3.2.1. Vasa

Vasa immunostaining, on sections at the level of the ovary central cavity, is clearly detectable in germ cells, located close in the germinal epithelium (Fig. 3a-d) or more deeply in the stroma (Fig. 3). The Vasa signal is very intense in oogonia, in the germinal epithelium and in groups inside the stroma, and the cytoplasmic labeling shows a quite uniform distribution (Fig. 3b-d). Also, groups of oocytes are recognizable for bigger dimensions and chromatin appearance (fainter and /or granular), when compared to oogonia (Fig. 3d, f). In previtellogenic oocytes located in the ovarian stroma and near the lumen, the anti-Vasa immunostaining is present in the whole cytoplasm, but it appears to weaken with oocyte growth, if compared to that of oogonia and early oocyte (Fig. 3d-f). However, previtellogenic oocytes have a particularly strong immunolabelling as a perinuclear ring very close to the nuclear envelope (Fig. 3b, d, f). In some cases, we observed characteristic structures that we named “plumes” for their shape (Fig. 3e) (see also Transmission Electron Microscopy section). Somatic follicular cells and somatic cells of the surrounding stroma result not labeled (es. Fig. 3e).

3.2.2. Tudor-containing proteins

In general, the labeling of Tudor proteins was fainter in comparison to Vasa immunostaining, consistent with the faint bands obtained in WB. Anti-TDRD7 labeling is visible in the germinal epithelium (Fig. 4a, b), it is very faint in oogonia (Fig. 4c), but it appears as clear cytoplasmic granules in the cytoplasm and cortical region of oocytes (Fig. 4a-c); immunostained granules increase in previtellogenic oocytes with size, and in bigger previtellogenic oocytes they are mainly concentrated in the perinuclear area (Fig. 4d). Anti-TDRKH labeling is observed in the germinal epithelium bordering the internal cavity (Fig. 4e, f). The labeling is visible in the cytoplasm of oogonia in the germinal epithelium (Fig. 4e, f) and in oogonia in the ovarian stroma (Fig. 4e). In previtellogenic oocytes the TDRKH immunostaining is present as small granules in the cytoplasm and as a few bigger spots in the perinuclear region very close to the nuclear membrane (Fig. 4e). The somatic cells of the ovarian stroma result unmarked (Fig. 4).

3.3. Immunolocalization of mitochondrial markers

Anti-TOMM20 labeling is differently distributed within the cytoplasm depending on the cell type (Fig. 5a, b). In oogonia the marking is diffused in the cytoplasm, while in oocytes it is present with greater intensity in the perinuclear area (Fig. 5b). In somatic cells of the connective tissue, anti-TOMM20 labeling is present as small granules uniformly distributed in the cytoplasm (Fig. 5a, b). The labeling with anti-PLD6 appears concentrated in large spots in oogonia and in oocytes, and, unlike anti-TOMM20, it is not visible in somatic cells of the ovary (Fig. 5c, d).

3.4. Transmission electron microscopy

The analysis of the ovary with TEM allowed us to observe at higher resolution electron-dense germ granules. We were interested in understanding if the bigger germ granules aggregated close to the nuclear envelope, as visualized by immunolocalization of germline factors, co-localize with mitochondria, supporting an interaction between germline determinants and mitochondria. Interestingly, in previtellogenic oocytes (Fig. 6a), we observed plumes made of piled mitochondria that depart from the perinuclear region in the ooplasm towards the oocyte plasma membrane and are intermingled with intermitochondrial cement, highly electron-dense granules located between the mitochondria (Fig. 6b-d). Also, electron-dense material, the so-called nuage, is localized close to nuclear pores and between the nuclear envelope and the mitochondrial aggregates (Fig. 6d, e), where broken mitochondria with exposed cristae, or almost empty mitochondrial membranes, are also visible (Fig. 6e). In bigger previtellogenic oocytes highly electron-dense granules remain close to the nuclear membrane, while mitochondrial plumes are no longer visible (Fig. 6f).

4. Discussion

Germline specification and differentiation remain one of the major fields of interest in developmental biology (Hansen and Pelegri, 2021; Yao et al., 2022). In this context, the aim of our study was to characterize the distribution patterns of evolutionarily conserved germline determinants together with the mitochondrial localization in female germ cells in the bony fish *P. reticulata*, a good new model animal for comparative biology studies with the most often analyzed zebrafish. Indeed, both *D. rerio* and *P. reticulata* have asynchronous ovary (Li and Ge, 2020), that shows, in transverse or longitudinal sections at the level of central lumen, multiple stages of germ cells scattered in the ovarian

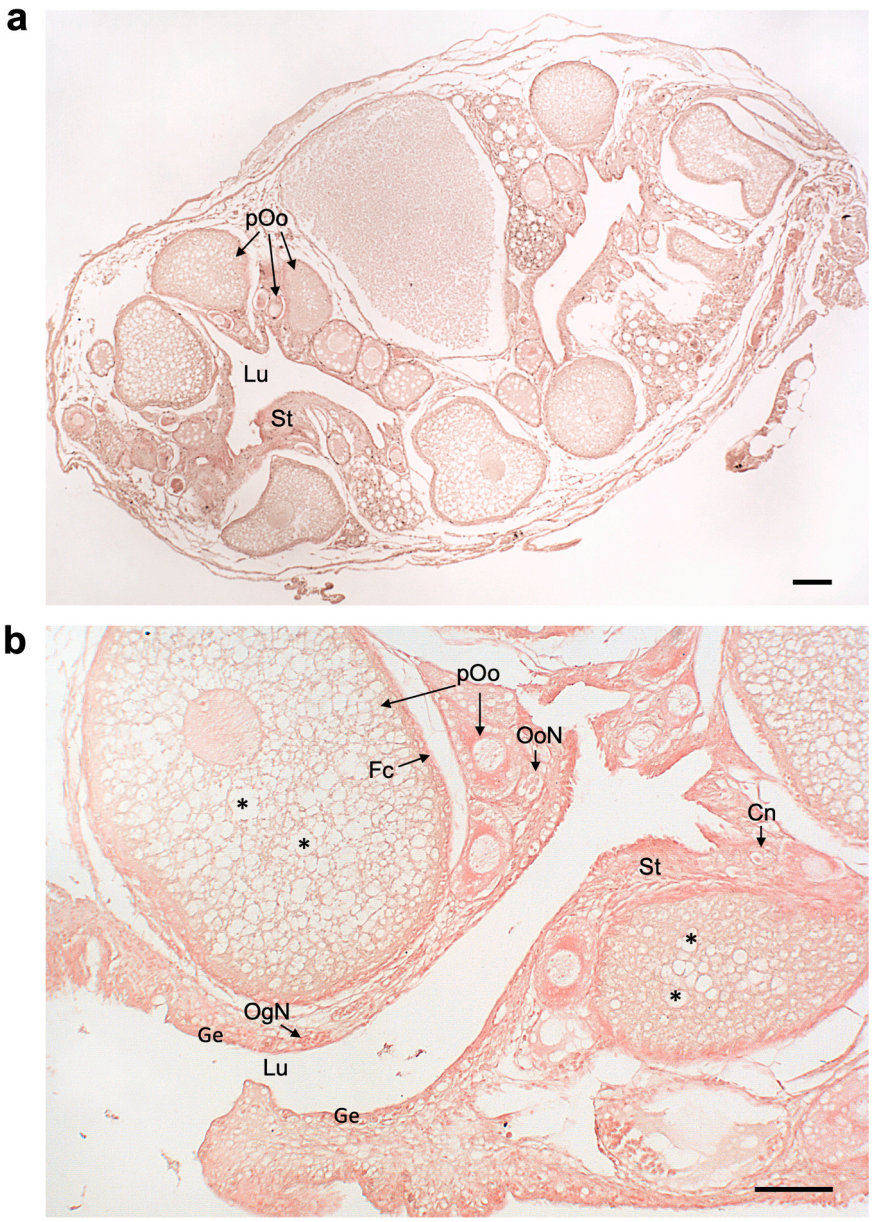

Fig. 2. Hematoxylin-eosin staining of an ovary longitudinal section. (a) Whole section. (b) Portion of a section at higher magnification, showing oocytes at different stages of growth. Lipid droplets (asterisks) are present. Acronyms: previtellogenic oocytes (pOo), ovarian lumen (Lu), ovarian stroma (St), germinal epithelium (Ge), nest of oogonia (OgN); nest of oocytes (OoN). The scale bar indicates 100 μm.

stroma (Elkouby and Mullins, 2017). At the same time, while *D. rerio* is an oviparous species, *P. reticulata* is viviparous. Many teleosts are oviparous, in which mature eggs are spawned into the aquatic environment where fertilization occurs. Viviparity, under which fish give birth to live offspring, is a less frequent reproductive mode and it can take many different forms depending on the species (Mokhtar, 2025). The presence of similarities and differences between zebrafish and the guppy makes in our opinion the comparison of the two species particularly interesting to be investigated further in the future for understanding the intermingled evolution of reproductive modes and germ cell differentiation.

Our aim was to investigate germ granules and mitochondrial relative distribution in oogonia and in previtellogenic oocytes at different growth stages. We instead removed vitellogenic oocytes because of yolk deposit, that prevented optimal sectioning and putative germ granule recognition. We used antibodies against germline markers for which there is evidence documenting their role in correct specification and differentiation of germ cells (the RNA helicase Vasa, and the Tudor proteins TDRD7 and TDRKH; reviewed in Seydoux and Braun, 2006; in *D. melanogaster*, Patil et al., 2014; in bovines, Tan et al., 2020). In addition, we immunolocalized TOMM20, a ubiquitous mitochondrial marker (e.g. in *D. rerio*, Arribat et al., 2019; in stem cells, Feng et al., 2021; in oocytes, Jin et al., 2022), and PLD6, a protein that has a role in mitochondrial dynamic during germ cell differentiation (e.g. in *M. musculus*, Watanabe et al., 2011; in *D. rerio*, Zhang et al., 2022).

The degree of conservation of the amino acid sequences of *H. sapiens* and the guppy suggested the correct immunodetection of *P. reticulata* homologs and the Western blot supported antibody specificity. Indeed, anti-Vasa, anti-TDRDKH and anti-TDRD7 antibodies showed bands with a molecular weight consistent with the predicted ones (~70 kDa and ~120 kDa, respectively). The additional band around 55 kDa, consistently found with Anti-TDRD7, supports the presence of two paralogs, as proposed in other teleosts, among which *D. rerio* and *Poecilia formosa* (Wang et al., 2019). We point out that in oocytes immunofluorescence

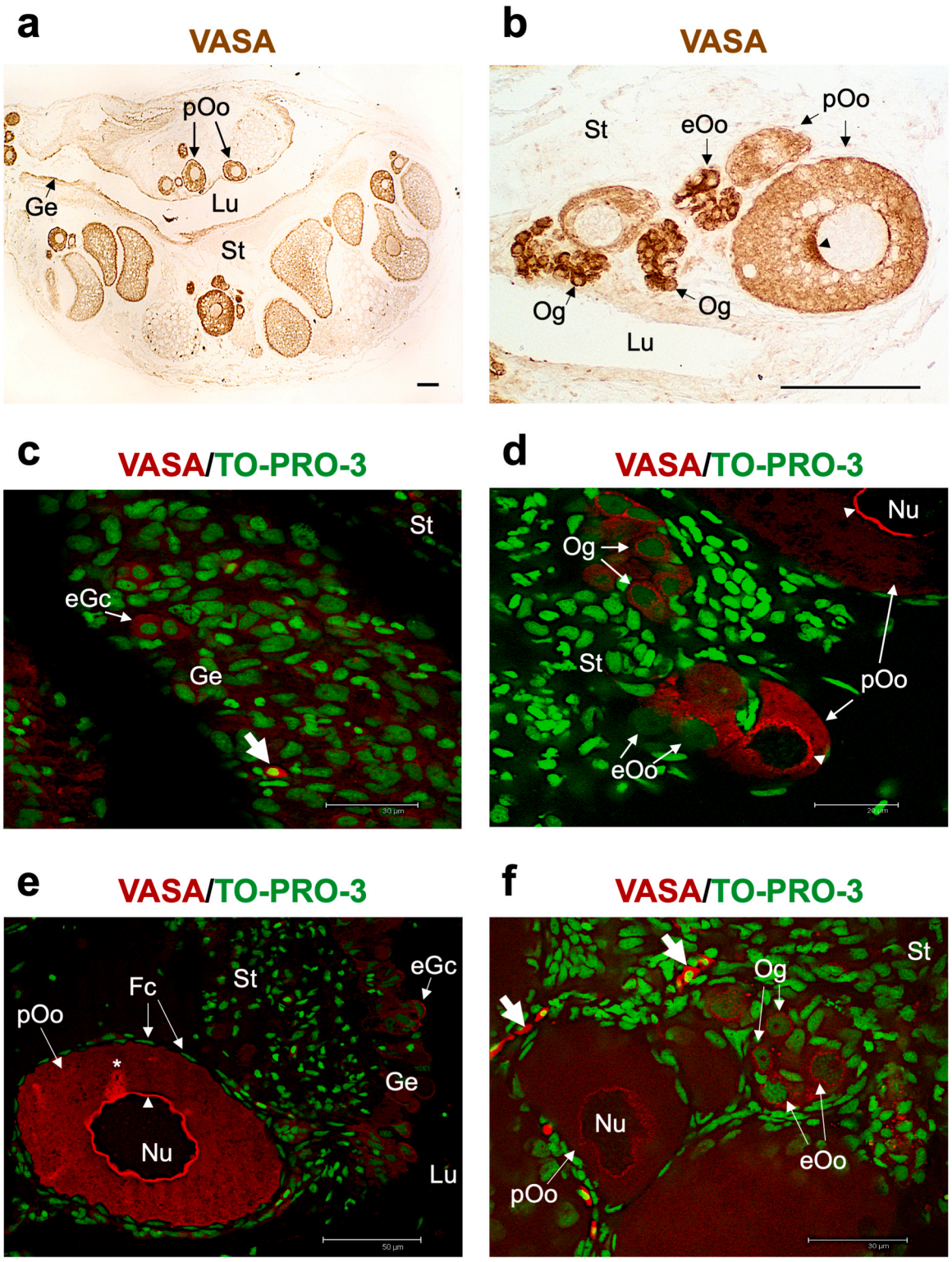

Fig. 3. Distribution of anti-Vasa labeling in sections of *Poecilia reticulata* ovary. (a, b) Immunohistochemistry of an ovary longitudinal section. Anti-Vasa labeling in brown. (a) The germinal epithelium around the ovary lumen resulted Vasa-labeled. Germ cells at different stages of differentiation are stained. (b) Oogonia and early oocytes show a strong cytoplasmic staining, that is fainter as oocytes grow; in previtellogenic oocytes a deeper concentration of the Vasa-labeling is present in the perinuclear region (arrowhead). (c-f) Immunofluorescence of portions of the ovary. Anti-Vasa labeling in red, nuclear dye in green. (c) Immunostaining is visible in early germ cell in the germinal epithelium. Erythrocytes (bold arrow) are stained. (d) Immunostaining is visible in oogonia and early and previtellogenic oocytes, with a stronger concentration of the Vasa-labeling (arrowhead) in the perinuclear region of the latter. (e) Immunostaining in early germ cell in the germinal epithelium. The immunolabeling in the perinuclear region of previtellogenic oocytes (arrowhead) is sometimes observed as plume-like structure (asterisk); follicular cells are not Vasa-stained. f) Immunostaining is visible in oogonia and early oocyte, with a stronger concentration of the Vasa-labeling in the perinuclear region of previtellogenic oocytes. Erythrocytes (bold arrow) are stained. Acronyms: previtellogenic oocytes (pOo), previtellogenic oocyte nucleus (Nu), early oocytes (eOo), follicular cells (Fc), ovarian lumen (Lu), somatic cells of the ovarian stroma (St), germinal epithelium (Ge), early germ cell (eGc), oogonia (Og). The scale bar indicates: a,b) 100 µm; c,f) 30 µm; d) 20 µm; e) 50 µm.

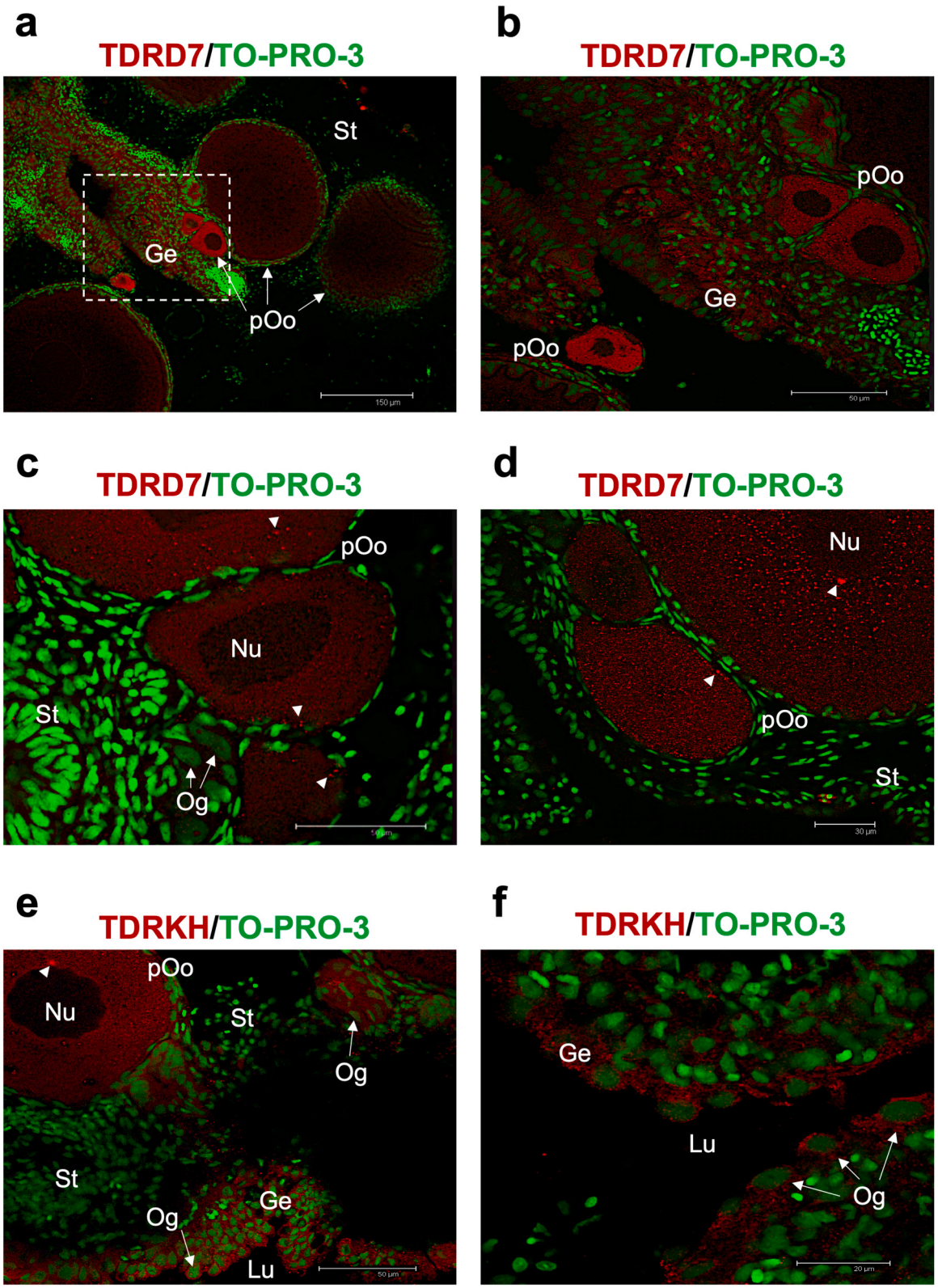

Fig. 4. Distribution of Tudor protein labeling in sections of *Poecilia reticulata* ovary. (a-d) Anti-TDRD7 in red, nuclear dye in green. (a, b) The labeling is clearly visible in the germinal epithelium and in previtellogenic oocytes. (b) is a magnification of the dashed area in (a). (c) The labeling is very faint in oogonia, but it appears as clear cytoplasmic granules in the cortical region of smaller previtellogenic oocyte. (d) The labeling shows a deeper concentration in the perinuclear region of bigger previtellogenic oocytes, where it forms big granules (arrowheads). No staining is visible in somatic cells of the ovarian stroma. (e, f) Anti-TDRKH in red, nuclear dye in green. (e) The labeling is observed in the germinal epithelium bordering the ovarian lumen. Oogonia in the germinal epithelium and stroma show a diffused cytoplasmic staining, while in previtellogenic oocytes the staining is present as small granules in the cytoplasm and as few bigger spots (arrowhead) close to the nuclear membrane. (f) Oogonia in the germinal epithelium show a diffused cytoplasmic staining. No staining is visible in somatic cells of the ovarian stroma. Acronyms: previtellogenic oocytes (pOo), ovarian lumen (Lu), somatic cells of the ovarian stroma (St), germinal epithelium (Ge), oogonia (Og), oocyte nucleus (Nu). The scale bar indicates: a) 150 µm; b,c,e) 50 µm; d) 30 µm; f) 20 µm.

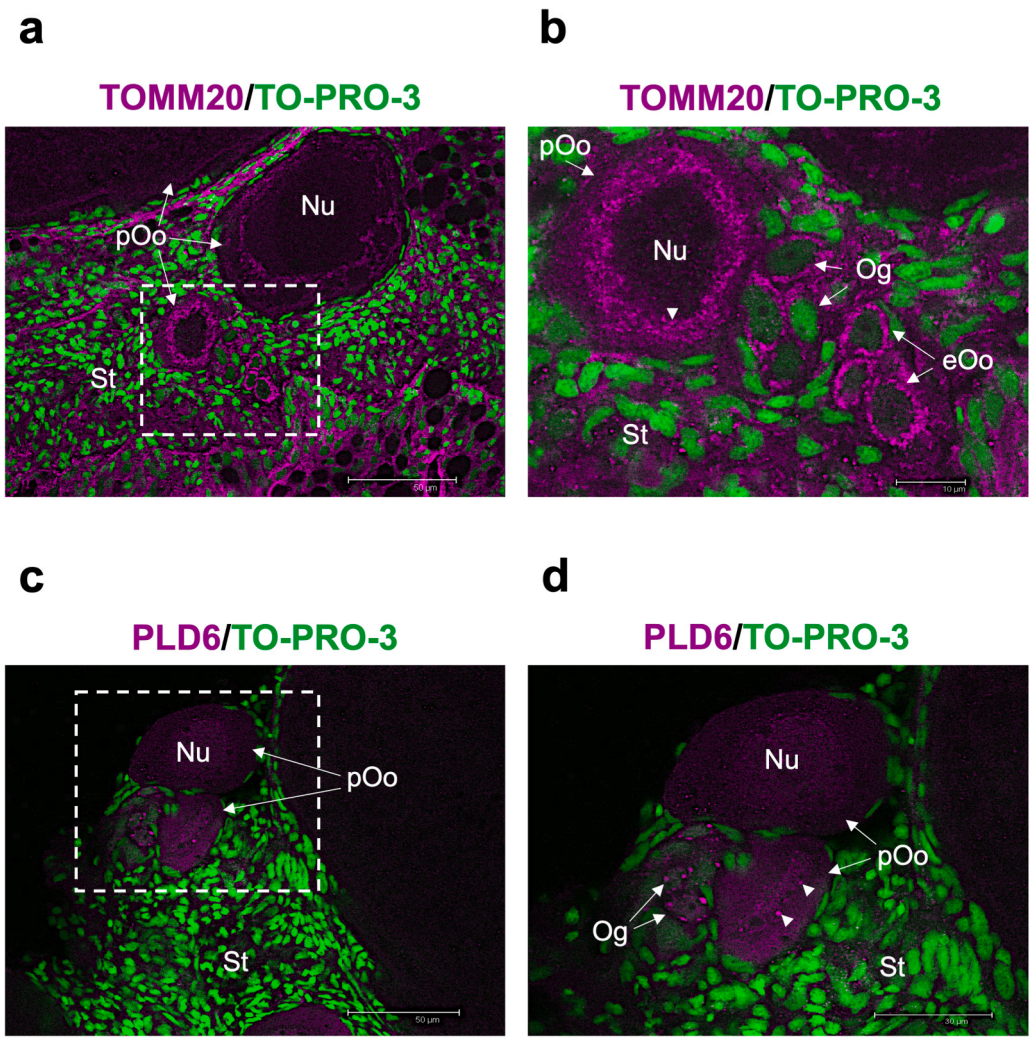

Fig. 5. Distribution of mitochondrial protein labeling in sections of *Poecilia reticulata* ovary. (a, b) Anti-TOMM20 labeling in magenta, nuclear dye in green. The number of stained mitochondria is higher in germ cells in comparison to somatic cells of the ovarian stroma. (b) Magnification of a portion of (a). In oogonia, stained mitochondria appear dispersed in the cytoplasm, while they are aggregated (arrowhead) all around the nuclear envelope in early oocyte and previtellogenic oocytes. (c, d) Anti-PLD6 labeling in magenta, nuclear dye in green. (c) PLD6-stained mitochondria appear as discrete aggregates around the nuclear envelope in oogonia and previtellogenic oocyte. (d) Magnification of a portion of (c) showing aggregation of mitochondria (arrowheads). Acronyms: oogonia (Og), early oocytes (eOo), previtellogenic oocytes (pOo), oocyte nucleus (Nu), somatic cells of the ovarian stroma (St). The scale bar indicates: a,c) 50 μm; b) 10 μm; d) 30 μm.

detection of Tudor proteins is much less than Vasa, while in testicular cysts these proteins are very abundant (data not shown); this can easily explain the faint bands detected in ovary homogenates when compared to WB male bands.

Anti-TOMM20 antibody showed a band ~20 kDa (predicted weight 16.47 kDa), while anti-PLD6 antibody showed a band around 55 kDa, therefore about double the expected weight for PLD6 (predicted weight 23.38 kDa). The latter suggests some kind of post-transcriptional and/or post-translation modification processing that deviates the molecular weight from the bioinformatic prediction based on nucleotide sequence translation. Since the band had a molecular weight almost twice the expected, another explanation could be a failure to dissociate the hydrogen-bonded dimeric active site of PLD6, even if the protocol applied involved protein denaturation. Nevertheless, these data, together with immunolocalization in tissues, support the specificity of the antibodies used.

The single ovary of *P. reticulata* is of cystovarian type, having an internal ovarian lumen, lined by germinal epithelium (Constantz, 1989; Lambert, 1970; Uribe et al., 2009; Uribe et al., 2010; Uribe et al., 2019). The mucosa of the ovarian wall forms ovarian lamellae into the lumen (Dodd, 1977; Selman and Wallace, 1989). As previously described in the literature, the germinal epithelium, besides somatic epithelial cells, also contains groups of oogonia and of early oocytes (i.e. germ cell nests) (Grier et al., 2007, 2009; Grier, 2012). Somatic epithelial cells are known to progressively surround individual oocytes and folliculogenesis is completed when the oocyte and its encompassing layer of somatic epithelial cells, now follicular cells, become surrounded by a vascularized theca (Grier, 2000; Grier et al., 2009). We observed groups of oogonia and oocytes (germ cell nests) close to the germinal epithelium; within the ovarian stroma, we observed previtellogenic follicles with oocytes in different stages of growth, recognizable by their dimension, position, and presence of lipid droplets (Uribe et al., 2019).

We observed anti-Vasa labeling in oogonia with a diffused cytoplasmic distribution, while oocytes showed a perinuclear labeling. Vasa is a component of perinuclear germ granules (e.g. in the viviparous teleost *Chapalichthys encaustus*, species of the Order Cyprinodontiformes, as *P. reticulata*, Guerrero-Estévez and Moreno-Mendoza, 2012) but documented also in other animals (e.g.,: the amphibian *R. clamitans*, Eddy, 1975).

Immunolocalization with anti-TOMM20 allowed us to observe an intense labeling with cytoplasmic distribution thickened in the perinuclear area from early oocyte stage onwards. TOMM20 is a ubiquitous

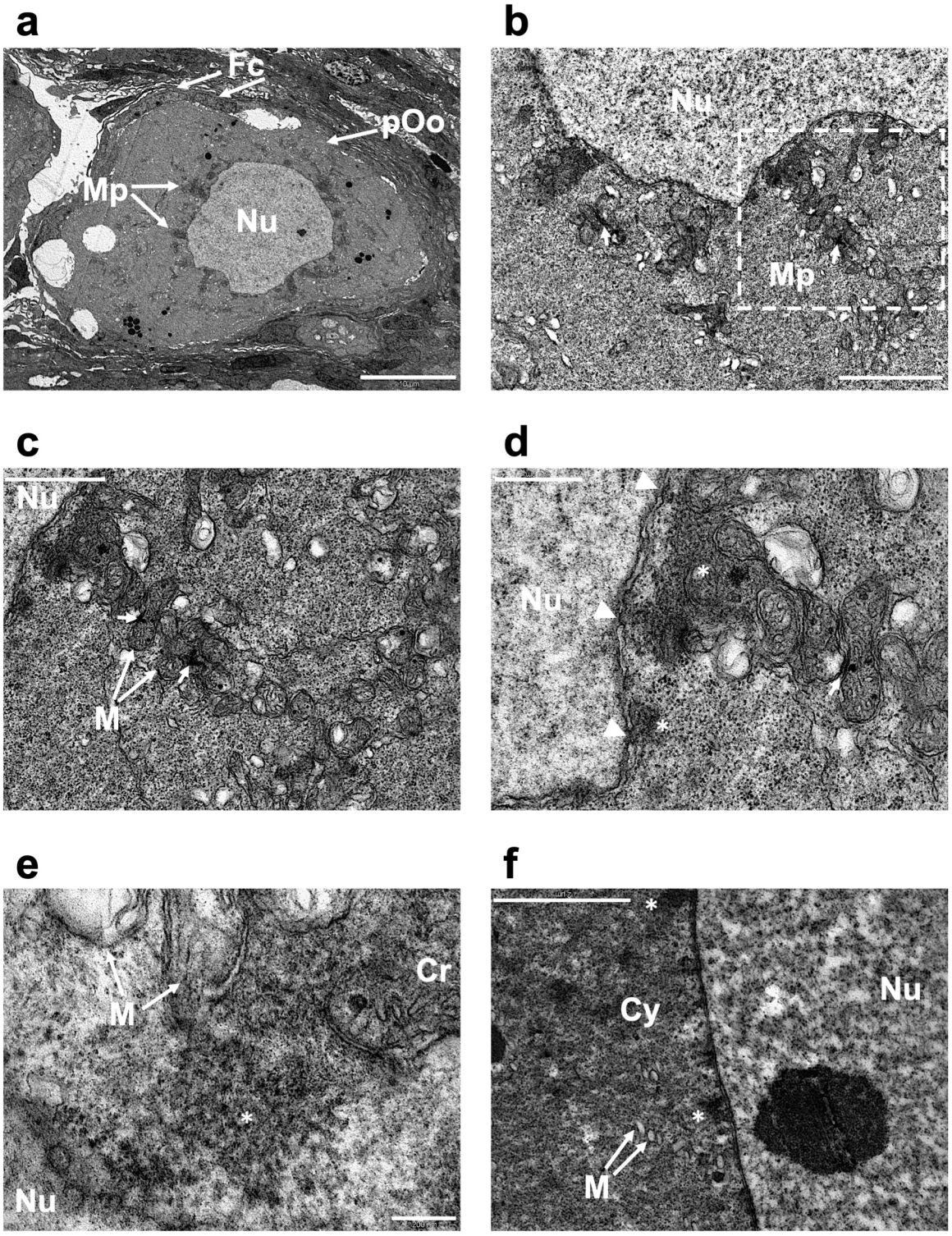

Fig. 6. Transmission electron microscopy images of *Poecilia reticulata* female germ cells. (a) Previtellogenic oocyte, surrounded by follicular cells, showing mitochondrial plumes departing from the perinuclear region towards the oocyte plasma membrane. (b) Magnification of (a), showing mitochondrial plumes with intermitochondrial cement (short arrows). (c) Magnification of (b). (d) Magnification of (c), electron-dense material (nuage) (asterisks) located between nuclear pores (arrowheads) and a mitochondrial plume with intermitochondrial cement (short arrows). (e) Region between the nuclear envelope and a mitochondrial aggregate. Perinuclear germ granules (asterisk) are close to empty mitochondria or broken mitochondria with extruded cristae. (f) Portion of an oocyte in a more advanced growth stage showing electron-dense granules (asterisks) along the nuclear envelope. No mitochondrial aggregate is visible, but a few "empty" mitochondrial membranes can be recognized. Acronyms: previtellogenic oocytes (pOo), oocyte nucleus (Nu), follicular cells (Fc), mitochondria (M), mitochondrial plumes (Mp), cristae near extruded mitochondrial material (Cr), cytoplasm (Cy). The scale bar indicates: a) 10 μm; b) 2 μm; c) 1 μm; d) 500 nm; e) 200 nm; f) 2 μm.

mitochondrial marker, therefore the distribution of anti-TOMM20 labeling is expected to provide information on the distribution of mitochondria within the cell. Components of the TOM complex have been shown in mammalian cell cultures to cluster in the mitochondrial membrane, with a density closely correlated to mitochondrial activity, being higher in mitochondria with higher membrane potential (Wurm et al., 2011). The strong anti-TOMM20 labeling in mitochondria concentrated in the oocyte perinuclear area can represent the intense respiratory activity required by these cells during meiosis, for example for the processing of mRNAs as soon as they exit the nucleus. With the onset of vitellogenesis, the deeply stained mitochondrial perinuclear aggregation appears to decrease, mirroring a decrease in energy demand as oocyte enters metabolic quiescence–a state of reversible growth arrest of the oocyte essential for its chromosomal stability and preservation (Kim and You, 2022). Our observations suggest that *P. reticulata* oocytes have a perinuclear distribution of TOMM20-rich mitochondria and Vasa-positive germ granules. The localization of mitochondria and germ granules within the same regions of the cell is supported by published data in many animals (e.g.: *Katharina tunicata*, *Rana pipiens* and *R. clamitans*, *Strongylocentrotus droebakhiensis*, Eddy, 1975; *Drosophila*, Amikura et al., 2001; sea urchins such as *Anthocidaris crassispina*, Reunov et al., 2001, Isaeva and Reunov, 2001; *M. musculus*, Reunov, 2006, Reunov and Reunova, 2015; *R. philippinarum*, Reunov et al., 2019, 2021), including other fish (e.g.: *Oryzias melastigma*, Reunov et al., 2020). Vasa has an RNA helicase activity that can promote the correct translation of mRNAs stored in germ granules around the nuclear membrane, such as the translation of factors needed for germ cell differentiation.

Anti-PLD6 labeling occurs as large granules in oogonia; the labeling appears to decrease as oogenesis proceeds. PLD6 is important in the regulation of mitochondrial dynamics during spermatogenesis in *Drosophila* and the mouse (Huang et al., 2011a; Chen et al., 2017) and in mammalian cell cultures (Schiavon et al., 2019). When PLD6 is overexpressed within a cell, phosphatidic acid synthesis increases, leading to mitochondrial aggregation (Chen et al., 2017). In the literature, PLD6 is generally considered a marker in both male (Huang et al., 2011a; Chen et al., 2017) and female germline (*D. rerio*, Zhang et al., 2022; *Drosophila*, Pane et al., 2007). Our observations in oogonia of large, anti-PLD6 labeled spots can represent the site of early germ granule formation, region of the cytoplasm in which mitochondrial opening during fission and fusion guided by PLD6 can promote mitochondrial material exit and recruitment into germ granules, as observed in *Drosophila* and sea urchin (Isaeva and Reunov, 2001) and in *R. philippinarum* (Reunov et al., 2019, 2021), and piRNA biogenesis (e.g.: in *D. melanogaster*, Nishimasu et al., 2012).

The Tudor proteins shared a localization in granules in the cytoplasm of oocytes, with a cytoplasmic staining from cortical to perinuclear during the progression of oocyte growth. Anti-TDRD7 labeling is not evident in oogonia, while in oocytes it appears in small spots. TDRD7 is important for the structural and functional integrity of germ granules (*D. melanogaster*, Arkov et al., 2006; zebrafish, Strasser et al., 2008). We can hypothesize that TDRD7 serves to assemble germ granules and stabilize them as scaffolding protein in oocytes throughout meiosis. Anti-TDRKH labeling is also present in oogonia in the germinal epithelium and in the stroma, and in previtellogenic oocytes it is localized in big aggregates very close to the nuclear envelope. Thus, TDRKH, Vasa, and active mitochondria share a perinuclear localization. We can suggest that these GMP proteins together with mitochondria act in the process of perinuclear germ granules organization, a ribonuclear protein platform for translational regulation and transposon silencing mediated by the piRNA pathway.

The most striking support to clustering of germ granules and mitochondria in the present study is the visualization at TEM of mitochondrial aggregate intermingled with electron-dense granular material in previtellogenic oocyte very close to the nuclear membrane. Previous immunocytochemical and ultrastructural analysis clearly documented the tight association of germ granules with nuclear pores, and TEM analysis showed what appeared to be material release from broken mitochondria in their proximity (e.g.: *Caenorhabditis elegans*, Pitt et al., 2000; *Mus musculus*, Reunov, 2006; *Ruditapes philippinarum*, Reunov et al., 2019). Given the result of the present study and the discussed bibliography, we support germ granules have both nuclear and mitochondrial origin, as proposed in other distantly related animals. Indeed, electron-dense material appears to exit nuclear pores close to the germ granules of mitochondrial plumes, where broken mitochondria, releasing electron-dense material, are also visible. In fish, accumulations of electron-dense material near the nuclei with mitochondria was previously documented (e.g.: the teleost *Chapalichthys encaustus*, Guerrero-Estévez and Moreno-Mendoza, 2012; *Oryzias latipes*, Kobayashi and Iwamatsu, 2000; *Sander lucioperca*, Żelazowska and Kujawa, 2022), as well as granules in the form of intermitochondrial cement (e.g.: *D. rerio*, Marlow and Mullins, (2008); *Labeobarbus marequensis*, Żelazowska and Halajian, 2020, or particular assembly of perinuclear nuage closely encircled by mitochondria (*Micropterus salmoides*, Żelazowska and Halajian, 2019; *Labeobarbus marequensis*, Żelazowska and Halajian, 2020), nonetheless, the peculiar ultrastructural morphology we observed, to our knowledge, has never been documented before. Indeed, we observed characteristic structures, that we named plumes for their shape, made up of aggregates of stacked mitochondria intermingled with electron-dense material that branch out from nuclear pores in a radial arrangement. Our observation enriched the many documented forms of germ-plasm related structures and underlines the co-participation of the nucleus and mitochondria in their production. In the future it will be interesting to adopt an immunological approach associated with TEM (iEM) to characterize the composition of *P. reticulata* perinuclear germ granules.

CRediT authorship contribution statement

Liliana Milani: Writing – original draft, Visualization, Supervision, Resources, Investigation, Funding acquisition, Conceptualization. **Maria Gabriella Maurizii:** Writing – original draft, Visualization, Supervision, Resources, Investigation, Funding acquisition, Conceptualization. **Valeria Franceschini:** Writing – review & editing, Visualization, Resources. **Pietro Cacialli:** Writing – review & editing, Visualization. **Maurizio Lazzari:** Writing – review & editing, Resources, Investigation. **Mariangela Iannello:** Writing – review & editing, Investigation. **Giovanni Piccinini:** Writing – review & editing, Investigation.

Declaration of Competing Interest

None.

Acknowledgment

We want to thank Maria Roberta Randi for TEM image acquisition, Simona Corneti for Lab management, Eleonora Poeta for protein quantification, and Gianni Oliveri and Laura Basile for their support during experimental procedures.

This study was supported by the Ricerca Fondamentale Orientata (RFO) funding from the University of Bologna to M.G.M. and to L.M.

References

Altschul, S.F., Gish, W., Miller, W., Myers, E.W., Lipman, D.J., 1990. Basic local alignment search tool. J. Mol. Biol. 215 (3), 403–410. https://doi.org/10.1016/S0022-2836(05)80360-2.

Amikura, R., Kashikawa, M., Nakamura, A., Kobayashi, S., 2001. Presence of mitochondria-type ribosomes outside mitochondria in germ plasm of *Drosophila* embryos. Proc. Natl. Acad. Sci. USA 98, 9133–9138. https://doi.org/10.1073/pnas.171286998.

Aravin, A.A., Chan, D.C., 2011. piRNAs meet mitochondria. Dev. Cell 20, 287–288. https://doi.org/10.1016/j.devcel.2011.03.003.

Arkov, A.L., Wang, J.Y., Ramos, A., Lehmann, R., 2006. The role of Tudor domains in germline development and polar granule architecture. Development 133, 4053–4062. https://doi.org/10.1242/dev.02572.

Arribat, Y., Grepper, D., Lagarrigue, S., Richard, J., Gachet, M., Philipp Gut, P., Amati, F., 2019. Mitochondria in embryogenesis: an organellogenesis perspective. Front. Cell Dev. Biol. 7. https://doi.org/10.3389/fcell.2019.00282.

Campuzano-Caballero, J.C., Uribe, M., 2014. Structure of the female gonoduct of the viviparous telost *Poecilia reticulata* (Poeciliidae) during nongestation and gestation stages. J. Morphol. 275, 247–257. https://doi.org/10.1002/jmor.20200.

Chen, Y., Liang, P., Huang, Y., Li, M., Zhang, X., Ding, C., Feng, J., Zhang, Z., Zhang, X., Gao, Y., Zhang, Q., Cao, S., Zheng, H., Liu, D., Songyang, Z., Huang, J., 2017. Glycerol kinase-like proteins cooperate with Pld6 in regulating sperm mitochondrial sheath formation and male fertility. Cell Discov. 3, 17030. https://doi.org/10.1038/celldisc.2017.30.

Chen, X., Zhu, Y., Zhu, T., Song, P., Guo, J., Zhong, Y., Gui, L., Mingyou Li, M., 2022. *Vasa* identifies germ cells in embryos and gonads of *Oryzias celebensis*. Gene 823, 146369. https://doi.org/10.1016/j.gene.2022.146369.

Constantz, D.G., 1989. Reproductive biology of the poeciliid fishes. In: Meffe, G.K., Snelson, F.F. (Eds.), Ecology and Evolution of Live Bearing Fishes (Poeciliidae). Prentice Hall, Englewood Cliffs, pp. 33–50.

D'Orazio, F.M., Balwierz, P.J., González, A.J., Guo, Y., Hernández-Rodríguez, B., Wheatley, L., Jasiulewicz, A., Hadzhiev, Y., Vaquerizas, J.M., Cairns, B., Lenhard, B., Müller, F., 2021. Germ cell differentiation requires Tdrd7-dependent chromatin and transcriptome reprogramming marked by germ plasm relocalization. e5 Dev. Cell 56, 641–656. https://doi.org/10.1016/j.devcel.2021.02.007.

Ding, D., Liu, J., Dong, K., Melnick, A.F., Latham, K.E., Chen, C., 2019. Mitochondrial membrane-based initial separation of MIWI and MILI functions during pachytene piRNA biogenesis. Nucleic Acids Res. 47, 2594–2608. https://doi.org/10.1093/nar/gky1281.

Dodd, J.M., 1977. The structure of the ovary of nonmammalian vertebrates. In: Zuckerman, S., Weir, B.J. (Eds.), The Ovary. Academic Press, New York, pp. 219–263.

Eddy, E.M., 1975. Germ plasm and the differentiation of the germ cell line. Int. Rev. Cytol. 43, 229–281. https://doi.org/10.1016/s0074-7696(08)60070-4.

Elkouby, Y.M., Mullins, M.C., 2017. Methods for the analysis of early oogenesis in Zebrafish. Dev. Biol. 430 (2), 310–324. https://doi.org/10.1016/j.ydbio.2016.12.014.

Ewen-Campen, B., Schwager, E.E., Extavour, C.G.M., 2010. The molecular machinery of germline specification. Mol. Reprod. Dev. 77, 3–18. https://doi.org/10.1002/mrd.21091.

Feng, X., Yin, W., Wang, J., Feng, L., Kang, Y.J., 2021. Mitophagy promotes the stemness of bone marrow-derived mesenchymal stem cells. Exp. Biol. Med. 246 (1), 97–105. https://doi.org/10.1177/1535370220964394.

Grier, H.J., 2000. Ovarian germinal epithelium and folliculogenesis in the common snook, *Centropomus undecimalis* (Teleostei: Centropomidae). J. Morphol. 243, 265–281. https://doi.org/10.1002/(SICI)1097-4687(200003)243:3<265::AID-JMOR4>3.0.CO;2-I.

Grier, H.J., 2012. Development of the follicle complex and oocyte staging in red drum, *Sciaenops ocellatus* Linnaeus, 1776 (Perciformes, Sciaenidae). J. Morphol. 273, 801–829. https://doi.org/10.1002/jmor.20034.

Grier, H.J., Uribe, M.C., Parenti, L.R., 2007. Germinal epithelium, folliculogenesis, and postovulatory follicles in ovaries of rainbow trout, *Oncorhynchus mykiss* (Walbaum, 1792) (Teleostei, Protacanthopterygii, Salmoniformes) (https://doi-org.ezproxy.unibo.it/). J. Morphol. 268, 293–310. https://doi.org/10.1002/jmor.10518.

Grier, H.J., Uribe, M.C., Patino, R., 2009. The ovary, folliculogenesis, and oogenesis in teleosts. In: Jamieson, B.G.M. (Ed.), Reproductive Biology and Phylogeny of Fishes (Agnathans and Bony Fishes). CRC Press, Boca Raton, pp. 25–84.

Gross-Thebing, T., Yigit, S., Pfeiffer, J., Reichman-Fried, M., Bandemer, J., Ruckert, C., Rathmer, C., Goudarzi, M., Stehling, M., Tarbashevich, K., Seggewiss, J., Raz, E., 2017. The vertebrate protein dead end maintains primordial germ cell fate by inhibiting somatic differentiation. Dev. Cell 43, 704–715.e5. https://doi.org/10.1016/j.devcel.2017.11.019.

Guerrero-Estévez, S., Moreno-Mendoza, N., 2012. Gonadal morphogenesis and sex differentiation in the viviparous fish *Chapalichthys encaustus* (Teleostei, Cyprinodontiformes, Goodeidae). J. Fish. Biol. 80, 572–594. https://doi.org/10.1111/j.1095-8649.2011.03196.x.

Hansen, C.L., Pelegri, F., 2021. Primordial germ cell specification in vertebrate embryos: phylogenetic distribution and conserved molecular features of preformation and induction. Front. Cell Dev. Biol. 9, 730332. https://doi.org/10.3389/fcell.2021.730332.

Hartung, O., Forbes, M.M., Marlow, F.L., 2014. Zebrafish *vasa* is required for germ-cell differentiation and maintenance. Mol. Reprod. Dev. 81 (10), 946–961. https://doi.org/10.1002/mrd.22414.

Houwing, S., Berezikov, E., Ketting, R.F., 2008. Zili is required for germ cell differentiation and meiosis in zebrafish. –2011 Embo J. 27, 2702. https://doi.org/10.1038/emboj.2008.204.

Houwing, S., Kamminga, L.M., Berezikov, E., Cronembold, D., Girard, A., van den Elst, H., Filippov, D.V., Blaser, H., Raz, E., Moens, C.B., Plasterk, R.H., Hannon, G.J., Draper, B.W., Ketting, R.F., 2007. A role for Piwi and piRNAs in germ cell maintenance and transposon silencing in Zebrafish. Cell 129, 69–82. https://doi.org/10.1016/j.cell.2007.03.026.

Huang, H., Gao, Q., Peng, X., Choi, S.Y., Sarma, K., Ren, H., Morris, A.J., Frohman, M.A., 2011a. piRNA-associated germline nuage formation and spermatogenesis require MitoPLD profusogenic mitochondrial-surface lipid signaling. Dev. Cell 20 (3), 376–387. https://doi.org/10.1016/j.devcel.2011.01.004.

Huang, H.Y., Houwing, S., Kaaij, L.J., Meppelink, A., Redl, S., Gauci, S., Vos, H., Draper, B.W., Moens, C.B., Burgering, B.M., Ladurner, P., Krijgsveld, J., Berezikov, E., Ketting, R.F., 2011b. Tdrd1 acts as a molecular scaffold for Piwi proteins and piRNA targets in zebrafish. Embo J. 30, 3298–3308. https://doi.org/10.1038/emboj.2011.228.

Isaeva, V.V., Reunov, A.A., 2001. Germ plasm and germ-line cell determination: the role of mitochondria. Russ. J. Mar. Biol. 27 (. 1), S8–S14.

Izumi, N., Shoji, K., Suzuki, Y., Katsuma, S., Tomari, Y., 2020. Zucchini consensus motifs determine the mechanism of pre-piRNA production. Nature 578, 311–316. https://doi.org/10.1038/s41586-020-1966-9.

Jin, X., Wang, K., Wang, L., Liu, W., Zhang, C., Qiu, Y., Liu, W., Zhang, H., Zhang, D., Yang, Z., Wu, T., Li, J., 2022. RAB7 activity is required for the regulation of mitophagy in oocyte meiosis and oocyte quality control during ovarian aging. Autophagy 18 (3), 643–660. https://doi.org/10.1080/15548627.2021.1946739.

Juliano, C.E., Swartz, S.Z., Wessel, G.M., 2010. A conserved germline multipotency program. Development 137, 4113–4126. https://doi.org/10.1242/dev.047969.

Kabayama, Y., Toh, H., Katanaya, A., Sakurai, T., Chuma, S., Kuramochi-Miyagawa, S., Saga, Y., Nakano, T., Sasaki, H., 2017. Roles of MIWI, MILI and PLD6 in small RNA regulation in mouse growing oocytes. Nucleic Acids Res. 45, 5387–5398. https://doi.org/10.1093/nar/gkx027.

Kim, J., You, Y.-J., 2022. Oocyte quiescence: from formation to awakening. Endocrinology 163, bqac049. https://doi.org/10.1210/endocr/bqac049.

Kobayashi, H., Iwamatsu, T., 2000. Development and fine structure of the yolk nucleus of previtellogenic oocytes in the medaka *Oryzias latipes*. Dev. Growth Differ. 42, 623–631. https://doi.org/10.1046/j.1440-169x.2000.00546.x.

Kobayashi, T., Kajiura-Kobayashi, H., Nagahama, Y., 2000. Differential expression of *vasa* homologue gene in the germ cells during oogenesis and spermatogenesis in a teleost fish, tilapia, *Oreochromis niloticus*. Mech. Dev. 99, 139–142. https://doi.org/10.1016/s0925-4773(00)00464-0.

Lambert, J.G.D., 1970. The ovary of the guppy *Poecilia reticulata*. The granulosa cells as sites of steroid biosynthesis. Gen. Comp. Endocrinol. 21, 287–304. https://doi.org/10.1016/0016-6480(70)90119-x.

Li, J., Ge, W., 2020. Zebrafish as a model for studying ovarian development: recent advances from targeted gene knockout studies. Mol. Cell. Endocrinol. 507, 110778. https://doi.org/10.1016/j.mce.2020.110778.

Marlow, F.L., Mullins, M.C., 2008. Bucky ball functions in Balbiani body assembly and animal-vegetal polarity in the oocyte and follicle cell layer in zebrafish. Dev. Biol. 321, 40–50. https://doi.org/10.1016/j.ydbio.2008.05.557.

Matova, N., Cooley, L., 2001. Comparative aspects of animal oogenesis. Dev. Biol. 231, 291–320. https://doi.org/10.1006/dbio.2000.0120.

Milani, L., Cinelli, F., Iannello, M., Lazzari, M., Franceschini, V., Maurizii, M.G., 2022. Immunolocalization of Vasa, PIWI, and TDRKH proteins in male germ cells during spermatogenesis of the teleost fish *Poecilia reticulata*. Acta Histochem. 124, 151870. https://doi.org/10.1016/j.acthis.2022.151870.

Mokhtar, D.M., 2025. Diversity and dynamics of fish ovaries: Insights into reproductive strategies, hormonal regulation, and ovarian development. Histol. Histopathol. 40, 283–295. https://doi.org/10.14670/HH-18-802.

Nishimasu, H., Ishizu, H., Saito, K., Fukuhara, S., Kamatani, M.K., Bonnefond, L., Matsumoto, N., Nishizawa, T., Nakanaga, K., Aoki, J., Ishitani, R., Siomi, H., Siomi, M.C., Nureki, O., 2012. Structure and function of Zucchini endoribonuclease in piRNA biogenesis. Nature 491, 284–287. https://doi.org/10.1038/nature11509.

Olsen, L.C., Aasland, R., Fjose, A., 1997. A *vasa*-like gene in zebrafish identifies putative primordial germ cells. Mech. Dev. 66, 95–105. https://doi.org/10.1016/s0925-4773(97)00099-3.

Pane, A., Wehr, K., Schupbach, T., 2007. Zucchini and squash encode two putative nucleases required for rasiRNA production in the *Drosophila* germline. Dev. Cell 12, 851–862. https://doi.org/10.1016/j.devcel.2007.03.022.

Patil, V.S., Anand, A., Chakrabarti, A., Kai, T., 2014. The Tudor domain protein Tapas, a homolog of the vertebrate Tdrd7, functions in piRNA pathway to regulate retrotransposons in germline of *Drosophila melanogaster*. BMC Biol. 12, 61. https://doi.org/10.1186/s12915-014-0061-9.

Pek, J.W., Anand, A., Kai, T., 2012. Tudor domain proteins in development. Development 139, 2255–2266. https://doi.org/10.1242/dev.073304.

Pitt, J.N., Schisa, J.A., Priess, J.R., 2000. P granules in the germ cells of caenorhabditis elegans adults are associated with clusters of nuclear pores and contain RNA. Dev. Biol. 219, 315–333. https://doi.org/10.1006/dbio.2000.9607.

Reunov, A., 2006. Structures related to the germ plasm in mouse. Zygote 14, 231–238. https://doi.org/10.1017/S0967199406003789.

Reunov, A., Alexandrova, Y., Komkova, A., Reunova, Y., Pimenova, E., Vekhova, E., Milani, L., 2021. VASA-induced cytoplasmic localization of CYTB-positive mitochondrial substance occurs by destructive and nondestructive mitochondrial effusion, respectively, in early and late spermatogenic cells of the Manila clam. Protoplasma 258, 817–825. https://doi.org/10.1007/s00709-020-01601-1.

Reunov, A., Alexandrova, Y., Reunova, Y., Komkova, A., Milani, L., 2019. Germ plasm provides clues on meiosis: the concerted action of germ plasm granules and mitochondria in gametogenesis of the clam *Ruditapes philippinarum*. Zygote 27, 25–35. https://doi.org/10.1017/S0967199418000588.

Reunov, A.A., Au, D.W.T., Alexandrova, Y.N., Au, D.W.T., Alexandrova, Y.N., Chiang, M.W.L., Wan, M.T., Yakovlev, K.V., Reunova, Y.A., Komkova, A.V., Cheung, N.K.M., Peterson, D.R., Adrianov, A.V., 2020. Germ plasm-related structures in marine medaka gametogenesis; novel sites of Vasa localization and the unique mechanism of germ plasm granule arising. Zygote 28 (1), 9–23. https://doi.org/10.1017/S0967199419000546.

Reunov, A., Isaeva, V., Au, D., Wu, R., 2001. Nuage constituents arising from mitochondria: Is it possible? Dev. Growth Differ. 42, 139–143. https://doi.org/10.1046/j.1440-169x.2000.00492.x.

Reunov, A.A., Reunova, Y.A., 2015. In mouse oocytes the mitochondrion-originated germinal body-like structures accumulate mouse Vasa homologue (MVH) protein. Zygote 23, 501–506. https://doi.org/10.1017/S0967199414000124.

Schiavon, C.R., Turn, R.E., Newman, L.E., Kahn, R.A., 2019. ELMOD2 regulates mitochondrial fusion in a mitofusin-dependent manner, downstream of ARL2. Mol. Biol. Cell 30, 1198–1213. https://doi.org/10.1091/mbc.E18-12-0804.

Selman, K., Wallace, R.A., 1989. Cellular aspects of oocyte growth in teleosts. Zool. Sci. 6, 211–231.

Seydoux, G., Braun, R.E., 2006. Pathway to totipotency: lessons from germ cells. Cell 127, 891–904. https://doi.org/10.1016/j.cell.2006.11.016.

Shinomiya, A., Tanaka, M., Kobayashi, T., Nagahama, Y., Hamaguchi, S., 2000. The *vasa*-like gene, *olvas*, identifies the migration path of primordial germ cells during embryonic body formation stage in the medaka, *Oryzias latipes*. Dev. Growth Diff. 42, 317–326. https://doi.org/10.1046/j.1440-169x.2000.00521.x.

Shrirao, A.B., Schloss, R.S., Fritz, Z., Shrirao, M.V., Rosen, R., Yarmush, M.L., 2021. Autofluorescence of blood and its application in biomedical and clinical research. Biotechnol. Bioeng. 118 (12), 4550–4576. https://doi.org/10.1002/bit.27933.

Shukalyuk, A.I., Isaeva, V.V., 2012. Molecular and sub-cellular gametogenic machinery of stem and germline cells across metazoa. In: Najman, S. (Ed.), Current Frontiers and Perspectives in Cell Biology. InTech, Rijeka, pp. 279–314. https://doi.org/10.5772/34896.

Siomi, M.C., Mannen, T., Siomi, H., 2010. How does the royal family of tudor rule the PIWI-interacting RNA pathway? Genes Dev. 24, 636–646. https://doi.org/10.1101/gad.1899210.

Strasser, M.J., Mackenzie, N.C., Dumstrei, K., Nakkrasae, L.-I., Stebler, J., Raz, E., 2008. Control over the morphology and segregation of Zebrafish germ cell granules during embryonic development. BMC Dev. Biol. 8, 58. https://doi.org/10.1186/1471-213X-8-58.

Tan, M., Tol, H.T.A.V., Rosenkranz, D., Roovers, E.F., Damen, M.J., Stout, T.A.E., Wu, W., Roelen, B.A.J., 2020. PIWIL3 forms a complex with TDRKH in mammalian oocytes. Cells 9 (6), 1356. https://doi.org/10.3390/cells9061356.

Tanaka, T., Hosokawa, M., Vagin, V.V., Reuter, M., Hayashi, E., Mochizuki, A.L., Kitamura, K., Yamanaka, H., Kondoh, G., Okawa, K., Kuramochi-Miyagawa, S., Nakano, T., Sachidanandam, R., Hannon, G.J., Pillai, R.S., Nakatsuji, N., Chuma, S., 2011. Tudor domain containing 7 (Tdrd7) is essential for dynamic ribonucleoprotein (RNP) remodeling of chromatoid bodies during spermatogenesis. Proc. Natl. Acad. Sci. USA 108, 10579–10584. https://doi.org/10.1073/pnas.1015447108.

Thomson, T., Lin, H., 2009. The biogenesis and function PIWI proteins and piRNAs: progress and prospect. Annu. Rev. Cell Dev. Biol. 25, 355–376. https://doi.org/10.1146/annurev.cellbio.24.110707.175327.

Uribe, M.C., Aguilar-Morales, M., De la Rosa-Cruz, G., Garcıa-Alarcon, A., Campuzano-Caballero, J.C., Guerrero-Estevez, S.M., 2010. Ovarian structure and embryonic traits associated with viviparity in poeciliids and goodeids. In: Uribe, M.C., Grier, H. J. (Eds.), Viviparous Fishes II. New Life Publications, Homestead, FL, pp. 211–229.

Uribe, M.C., De la Rosa Cruz, G., García Alarcón, A., Campuzano Caballero, J.C., Guzmán Bárcenas, M.G., 2019. Structures associated with oogenesis and embryonic development during intraovarian gestation in viviparous teleosts (Poeciliidae). Fishes 4, 35. https://doi.org/10.3390/fishes4020035.

Uribe, M.C., Grier, H.J., De la Rosa Cruz, G., Garcıa Alarcon, A., 2009. Modifications in ovarian and testicular morphology associated with viviparity in teleosts. In: Jamieson, B. (Ed.), Reproductive Biology and Phylogeny of Fish (Agnatha and Osteichthyes). Science Publishers, Enfield, NH, U.S.A, pp. 85–117.

Voronina, E., Seydoux, G., Sassone-Corsi, P., Nagamori, I., 2011. RNA granules in germ cells. Cold Spring Harb. Perspect. Biol. 3, a002774. https://doi.org/10.1101/cshperspect.a002774.

Wang, M., Ding, H., Wu, S., Wang, M., Wei, C., Wang, B., Bao, Z., Hu, J., 2022. Vasa Is a potential germ cell marker in leopard coral grouper (*Plectropomus leopardus*). Genes 13, 1077. https://doi.org/10.3390/genes13061077.

Wang, B., Du, X., Wang, H., Jin, C., Gao, C., Liu, J., Zhang, Q., 2019. Comparative studies on duplicated *tdrd7* paralogs in teleosts: molecular evolution caused neo-functionalization. Comp. Biochem. Physiol. D. Genom. Proteom. 30, 347–357. https://doi.org/10.1016/j.cbd.2019.04.006.

Watanabe, T., Chuma, S., Yamamoto, Y., Kuramochi-Miyagawa, S., Totoki, Y., Toyoda, A., Hoki, Y., Fujiyama, A., Shibata, T., Sado, T., Noce, T., Nakano, T., Nakatsuji, N., Lin, H., Sasaki, H., 2011. MITOPLD is a mitochondrial protein essential for nuage formation and piRNA biogenesis in the mouse germline. Dev. Cell 20, 364–375. https://doi.org/10.1016/j.devcel.2011.01.005.

Wurm, C.A., Neumann, D., Lauterbach, M.A., Harke, B., Egner, A., Hell, S.W., Jakobs, S., 2011. Nanoscale distribution of mitochondrial import receptor Tom20 is adjusted to cellular conditions and exhibits an inner-cellular gradient. Proc. Natl. Acad. Sci. USA 108 (33), 13546–13551. https://doi.org/10.1073/pnas.1107553108.

Yao, C., Yao, R., Luo, H., Shuai, L., 2022. Germline specification from pluripotent stem cells. Stem Cell Res. Ther. 13, 74. https://doi.org/10.1186/s13287-022-02750-1.

Żelazowska, M., Halajian, A., 2019. Previtellogenic oocytes of South African largemouth bass *Micropterus salmoides* Lacépède 1802 (Actinopterygii, Perciformes) - the Balbiani body, cortical alveoli and developing eggshell. J. Morphol. 280, 360–369. https://doi.org/10.1002/jmor.20948.

Żelazowska, M., Halajian, A., 2020. Asymmetry in the cytoplasm of oocytes of largescale yellowfish *Labeobarbus marequensis* Smith 1841 (Teleostei: Cypriniformes: Cyprinidae). J. Morphol. 281, 997–1009. https://doi.org/10.1002/jmor.21228.

Żelazowska, M., Kujawa, R., 2022. Microscopic study of the primary growth ovarian follicles of the pike-perch *Sander lucioperca* (Linnaeus 1758) (Actinopterygii, Perciformes). Micron 160C, 103318. https://doi.org/10.1016/j.micron.2022.103318.

Zhang, R., Tu, Y.X., Ye, D., Gu, Z., Chen, Z.X., Sun, Y.A., 2022. A germline-specific regulator of mitochondrial fusion is required for maintenance and differentiation of germline stem and progenitor cells. Adv. Sci. 9, 2203631. https://doi.org/10.1002/advs.202203631.

Zhou, L., Wang, X., Du, S., Wang, Y., Zhao, H., Du, T., Yu, J., Wu, L., Song, Z., Liu, Q., Li, J., 2020. Germline specific expression of a vasa homologue gene in the viviparous fish black rockfish (*Sebastes schlegelii*) and functional analysis of the vasa 3′ untranslated region. Front. Cell Dev. Biol. 8, 575788. https://doi.org/10.3389/fcell.2020.575788.